Feasible Dispatch Limits of PV Generation with Uncertain Interconnection of EVs in the Unbalanced Distribution Network

Mohammad Ramin Feizi, Student Member, IEEE, Mohammad E. Khodayar, Senior Member, IEEE, Bo Chen, Member, IEEE

Abstract—This paper presents a framework to determine the feasible dispatch limits of solar photovoltaic (PV) generation in the unbalanced distribution network considering the interconnection of electric vehicles (EVs) and associated uncertainties. The proposed framework determines the lower and upper dispatch limits of PV generation considering the worst-case realization of a) the minimum and maximum storage capacity of EVs, b) the minimum and maximum power dispatch of EVs, c) the lower and upper bounds for the arrival and departure times, and d) the available energy at arrival and departure times. The unbalanced operation of the distribution network as well as the uncertainty in the maximum PV generation and demand forecasts were considered. The problem formulation and solution approach are validated using the modified IEEE 34-bus and IEEE 123-bus distribution systems. The impacts of the budget of uncertainty and the vehicle-to-grid operation mode of EV clusters were addressed in the case studies. It is shown that integrating EVs with charging capability will increase the lower dispatch limit or increase the upper dispatch limit of the PV generation. Moreover, the increase in the budget of uncertainty will reduce the difference between the upper and lower dispatch limits by increasing the lower dispatch or decreasing the upper dispatch limit of the PV generation. Finally, it is shown that the vehicleto-grid capability will reduce the total lower dispatch limit or increase the total upper dispatch limit of the PV generation in the operation horizon.

Index Terms—dispatchable limit, electric vehicle, solar PV generation.

Nomenclature

A. Sets and Indices:

m

b	Index of bus.
d	Index of demand.
e	Index of electric vehicle cluster.
i	Index of distributed generation.
l	Index of distribution branch.
n	Index of distribution feeder.
v	Index of PV generation unit.

Index of scenario.

Mohammad Ramin Feizi and Mohammad E. Khodayar are with the Department of Electrical and Computer Engineering, Southern Methodist University, Dallas, TX 75205 USA (email: mfeizi@smu.edu, mkhodayar@smu.edu). Bo Chen is with the Energy Systems Division, Argonne National Laboratory, Lemont, IL 60439 USA (email: bo.chen@anl.gov)

This work was supported by National Science Foundation under Grant ECCS-1710923 and U.S. Department of Energy's Office of Energy Efficiency and Renewable Energy (EERE) under the Solar Energy Technologies Office Award Number 34230.

ϕ	Index of phase.
t	Index of time.

B. Variables:

 $\begin{matrix} l_{v,t}^{\phi,m} \\ u_{v,t}^{\phi,m} \end{matrix}$

$v, \iota_{_{_{l}}}$	-11
$IA_{e,t}^{\phi,m}$	Binary variable indicating the arrival of EV
4	cluster e on phase ϕ in scenario m .
$IC_{e,t}^{\phi,m}$	Interconnection of EV cluster e on phase ϕ to
4 /	the distribution network.
$IC_{e,t}^{A,\phi,m}$	Auxiliary binary variable to determine the
D /	connectivity of EV clusters.
$IC_{e,t}^{D,\phi,m}$	Auxiliary binary variable to determine the
4	connectivity of EV clusters.
$ID_{e,t}^{\phi,m}$	Binary variable indicating the departure of EV
4	cluster e on phase ϕ in scenario m .
$E_{e,t}^{\phi,m}$	Energy stored in an EV cluster.
$P_{(.),t}^{\overrightarrow{\phi},m}$	Real power of a unit on phase ϕ at time t .
$P_{(.),t}^{\phi,m}$ $P_{e,t}^{\phi,m,ch}$	Charging power of an EV cluster.
$P_{e,t}^{\phi,m,dc}$	Discharging power of an EV cluster.
$Q_{(.),t}^{\phi,m}$	Reactive power of a unit on phase ϕ at time t .
$PL_{l,t}^{\phi,m}$	Real power flow of branch l .
$QL_{l,t}^{\varphi,m}$	Reactive power flow of branch l .
$s_{b,t}^{(.),\phi,m}$	Positive slack variable.
$SL_{l,t}^{\phi,m}$	Apparent power flow of branch l .
$SL_{l,t}^{\phi,m} \ oldsymbol{U}_{b,t}^{m}$	Squared bus voltage vector in scenario m .
$\delta_{e,t}^{\phi,m}$	Auxiliary binary variable representing the
0,0	uncertainty in minimum energy storage
	capacity of EV cluster e connected to phase ϕ .
$\gamma_{e,t}^{\phi,m}$	Auxiliary binary variable representing the
- /-	uncertainty in maximum energy storage
,	capacity of EV cluster e connected to phase ϕ .
$\beta_{e,t}^{\phi,m,arv}$	Auxiliary binary variable representing the
	uncertainty in available energy storage of EV
	cluster e connected to phase ϕ at arrival time.
$\beta_{e,t}^{\phi,m,dep}$	Auxiliary binary variable representing the
	uncertainty in available energy storage of EV
	cluster e connected to phase ϕ at departure
.	time.
$\mu_{e,t}^{\phi,m,ch}$	Auxiliary binary variable representing the
	uncertainty in charging power of EV cluster e
	connected to phase ϕ .

Lower limit for PV generation v.

Upper limit for PV generation v.

$ au_e^{\phi,m,arv}$	Auxiliary binary variable representing the
	uncertainty in the arrival time of EV cluster
	e connected to phase ϕ .
$ au_e^{\phi,m,dep}$	Auxiliary binary variable representing the
	uncertainty in the departure time of EV cluster
	e connected to phase ϕ .
$\mu_{e.t}^{\phi,m,dc}$	Auxiliary binary variable representing the
. 0,0	uncertainty in discharging power of EV cluster
	e connected to phase ϕ .
$c_t^{\phi,m}$	Auxiliary variable representing the time
-	sequence.
$T_e^{\phi,m,arv}$	Arrival time for EV cluster e .
$T_e^{\phi,m,arv} \ T_e^{\phi,m,dep}$	Departure time for EV cluster e .
Ü	-

C. Parameters:

 $\hat{P}_e^{\phi,dc,max}$

 $\widetilde{P}_{e}^{\phi,ch,max}$

 $\widetilde{P}^{\phi,dc,max}$

 $IR_{v,t}^m$

A_v^ϕ	Area covered by the solar PV cells \boldsymbol{v} connected
	to phase ϕ .
$AD_{d,b}$	Element of demand-bus incidence matrix.
$AE_{e,b}$	Element of energy storage-bus incidence
-,-	matrix.
$AI_{i,b}$	Element of unit-bus incidence matrix.
$AL_{l,b}$	Element of line-bus incidence matrix.
$AV_{v,b}$	Element of PV-bus incidence matrix.
$AN_{n,b}$	Element of feeder-bus incidence matrix.
$\hat{E}_e^{\phi,min}$	The lower uncertainty bound for the minimum
L_e	available energy for EV cluster e on phase ϕ .
$\hat{E}_e^{\phi,max}$	
$E_e^{ au,\cdots}$	The lower uncertainty bound for the maximum
~ min	available energy for EV cluster e on phase ϕ .
$\widetilde{E}_e^{\phi,min}$	The difference between the lower and upper
	uncertainty bounds for the minimum available
~ .	energy for EV cluster e on phase ϕ .
$\widetilde{E}_e^{\phi,max}$	The difference between the lower and upper
	uncertainty bounds for the maximum available
	energy for EV cluster e on phase ϕ .
$\hat{l}_e^{\phi,arv}$	The lower uncertainty bound for the available
-	energy at arrival time.
$\hat{l}_e^{\phi,dep}$	The lower uncertainty bound for the available
Ü	energy at departure time.
$\widetilde{l}_e^{\phi,arv}$	The difference between the lower and upper
Ü	uncertainty bounds for available energy at
	arrival time.
$\widetilde{l}_e^{\phi,dep}$	The difference between the lower and upper
Ü	uncertainty bounds for available energy at
	departure time.
^ / T	- r · · · · · · · · · · · · · · · · · ·

The lower uncertainty bound for the maximum charging power for EV cluster e on phase ϕ .

The lower uncertainty bound for the maximum

discharging power for EV cluster e on phase

The difference between the lower and upper

uncertainty bounds for the maximum charging

The difference between the lower and

upper uncertainty bounds for the maximum

discharging power of EV cluster e on phase ϕ .

Solar radiation converted to electricity by the

PV solar generation v at time t in scenario m.

power of EV cluster e on phase ϕ .

	distribution network $(p_l^{\phi} \in \boldsymbol{p}_l)$.
$SL_l^{\phi,max}$	Apparent power capacity of branch l .
$P_{(.)}^{\phi,max}$ $Q_{(.)}^{\phi,max}$	Maximum real power of a unit on phase ϕ .
$Q_{(.)}^{\phi,max}$	Maximum reactive power of a unit on phase ϕ .
$S_{(.)}^{(.)}^{(.)}$	Maximum apparent power of a unit on phase ϕ .
PF_n	Acceptable power factor at distribution feeder
	n.
$\hat{T}_e^{\phi,arv}$	Forecasted arrival time for EV cluster e
$\hat{T}_e^{\phi,dep}$	connected to phase ϕ . Forecasted departure time for EV cluster e
$\widetilde{T}_e^{\phi,arv,min}$	connected to phase ϕ . The lower uncertainty bound for the arrival
$\widetilde{T}_e^{\phi,arv,max}$	time of EV cluster e connected to phase ϕ . The upper uncertainty bound for the arrival time of EV cluster e connected to phase ϕ .
$\widetilde{T}_e^{\phi,dep,min}$	The lower uncertainty bound for the departure
$\widetilde{T}_e^{\phi,dep,max}$	time of EV cluster e connected to phase ϕ . The upper uncertainty bound for the departure
$\Lambda^{\phi,arv}$	time of EV cluster e connected to phase ϕ . Budget of uncertainty for arrival time on phase
$\Lambda^{\phi,dep}$	ϕ . Budget of uncertainty for departure time on
$\Gamma^{\phi,E_{min}}$	phase ϕ . Budget of uncertainty for minimum energy capacity in EV clusters connected to phase ϕ .
$\Gamma^{\phi,E_{max}}$	Budget of uncertainty for maximum energy
$\Gamma^{\phi,ch}$	capacity in EV clusters connected to phase ϕ . Budget of uncertainty for charging power
$\Gamma^{\phi,dc}$	capacity of EV clusters connected to phase ϕ . Budget of uncertainty for discharging power
$\Gamma^{\phi,arv}$	capacity of EV clusters connected to phase ϕ . Budget of uncertainty for available energy in EV clusters connected to phase ϕ at arrival
$\Gamma^{\phi,dep}$	time. Budget of uncertainty for available energy in EV clusters connected to phase ϕ at departure
η^e_{ch}	time. Charging efficiency of EV cluster e .

Vector of available phases on the branch l in

 \boldsymbol{p}_l

 η_{dc}^e NT

I. INTRODUCTION

Total simulation period.

Discharging efficiency of EV cluster e.

OLAR power generation is the fastest growing renewable resource which is expected to provide a quarter of global electricity needs and reduce the global CO₂ emission of the energy sector by 21% by 2050 [1]. Lowering the energy costs, reducing the carbon footprint of energy supply to electric vehicles (EVs), and mitigating the reliance on fossil fuel resources to generate the electricity required to charge EVs, are among the motivations to leverage PV generation for EV charging. The global deployment of EV technology has been growing rapidly in the last decade and the number of passenger EVs increased by 63% in 2018 compared to the previous year worldwide [2]. The increase in the installed capacity of PV generation as the power supply, and the growing

market of EVs as electric loads with storage capability, introduce operational challenges to the power grid operators. Considering the uncertainties in the PV generation and EV interconnections in the distribution networks, managing the demand and supply to ensure reliability and network security is a challenging task. This paper presents a framework to determine the feasible dispatch limits of PV generation that ensure the security of the distribution network considering the uncertainty in the EV interconnection. The organization of this section is as follows: first, the motivation of this research is presented, later the existing literature in this domain is discussed and the contribution of the paper is highlighted. Finally, the organization of this paper is presented.

A. Motivation of research

The increase in EV sales and improvements to the EV battery capacity will reshape the electricity demand in the distribution networks. The changes in the distribution network demand profile stemming from integrating fast charging and commercial vehicle charging stations, and residential EV charging hubs introduce operational challenges in network security and reliability. The increase in the demand as a result of charging EVs increases the network loss, deteriorates the power quality with considerable voltage drops, and increases the stress on power distribution assets. In this context, effective coordination among the EV operators and other distributed energy resources would address the challenges imposed by EVs in the distribution networks.

Among distributed energy resources, solar PV generation has the largest penetration in the distribution networks. Rooftop solar PV panels and utility-scale solar plants improve the reliability and economics of energy supply as such energy resources could be placed close to the consumers in the distribution networks. Serving the EVs with solar PV generation would further reduce the carbon footprint of the energy supply chain for EVs. The integration of solar PV in the distribution network introduces several challenges including voltage fluctuations, voltage imbalances, reverse power flow, and protection devices' malfunctions. Coordinating the PV generation with EV charging/discharging could mitigate the adverse effects of PV generation in the distribution networks.

Given the limitations of the current assets in serving the growing EV demand and the current investment portfolio on solar PV generation resources in distribution networks, quantifying the dispatchable limits of PV generation is crucial to maintain the security of the distribution network. Quantifying the dispatchable PV generation enables the distribution system operator to gain an understanding of the feasible dispatch limits of this generation resource to avoid voltage violations and demand curtailments. The uncertainties associated with the EV integration, including the arrival and departure times and the stochasticity in energy and power capacity limits, are represented as the uncertainties in demand and available energy storage capacity in the distribution network. Motivated by such notions, this research is focused on determining the feasible dispatch limits of PV generation

with the uncertain interconnection of EVs in the distribution network.

B. Background and related works

The integration of EV in distribution system operation was addressed in [3]-[7]. In [3], the chargeable region for EVs was quantified by formulating a two-stage robust optimization problem with the network's technical constraints. The impacts of charging EVs on the distribution network were evaluated in [5] considering the uncertainties in the EVs' ownership, rating, and duration of charging as well as the distributed generation (DG) penetration. As high penetration of EVs in the distribution network impacts the operational and technical measures including power loss, nodal voltage profile, and operation cost; ensuring the reliability and security of the distribution network imposes capacity limits on the EV demand served in the distribution network. An approach to allocating the EV parking lots and renewable energy resources was presented in [6] that minimizes the loss in the distribution network. Meta-heuristic approaches are used to minimize the loss in the distribution network. An online adaptive EV charging strategy was proposed in [7] to minimize the voltage imbalances and violations, transformer capacity violations, and EV charging cost, while considering the EV owners' convenience.

Earlier research quantified and improved the PV hosting capacity in the distribution networks. The impacts of PV generation capacity on the maximum voltage of the feeder and line loading along the feeder were investigated in [8] considering various demand profiles. Voltage regulation was used in [9] to improve the hosting capacity of PV generation in the distribution network. The harmonics injected by distributed generation and demand could reduce the hosting capacity of solar PV in the distribution network. Passive filters were designed in [10] to address this challenge, minimize the loss and maximize the power factor. In [11] the hosting capacity of PV generation was maximized using network management strategies including topology reconfiguration, capacitor switching, and voltage regulation. Monte Carlo simulation was used to determine PV deployment scenarios and power flow was used to evaluate possible violations in voltage and current constraints. In [12], an approach to determine the dynamic operation set points of the energy storage was proposed to mitigate the overvoltage in distribution networks with high penetration of PV generation. In [13], voltage droop control was used in transformers to improve the PV hosting capacity in the distribution network by increasing the voltage variation boundaries. In [14], the PV hosting capacity of the distribution network was quantified using a stochastic framework that leverages Monte Carlo simulation to determine the PV deployment scenarios. An algorithm to quantify the hosting capacity of PV generation in a distribution network was presented in [15]. Monte Carlo simulation was incorporated to procure the PV deployment scenarios and time-series power flow simulation was used to determine the nodal voltages and evaluate network constraint violations. An approach for allocating the series and shunt

voltage source converters was introduced in [16] to improve the hosting capacity of PV generation in distribution networks. In [17] the hosting capacity of PV generation was improved by regulating the heating and cooling loads of the customers in the distribution network. A distributed framework using Dantzig-Wolfe decomposition was proposed to address the consumers' privacy. An approach to determine the PV hosting capacity of the distribution network was proposed in [18] considering the smart inverter control strategies for the PV generation and battery energy storage. PV hosting capacity is evaluated using an interval overvoltage probability-based approach to decrease the risk associated with voltage violations in [19] while considering the uncertainty in PV generation and demand.

The integration of EV in the distribution network impacts the hosting capacity of PV generation. Earlier research addressed the interactions between EV and PV technologies in the three-phase balanced [20]-[24] and unbalanced [25]-[27] distribution networks. In [20] the authors proposed a conceptual framework to investigate the large-scale integration of solar PV generation and EVs, considering the coordination among these assets with multiple EV penetration levels. To reduce the solar PV curtailment and customer costs, [21] proposed an EV charging management scheme using an auction mechanism that captured the benefit and voluntary participation of each customer. A two-stage operation framework for the EV parking stations with rooftop solar PV generation was proposed in [22] to schedule the EV charging in the day-ahead and real-time operations, considering the uncertainties in the available solar power generation and customer parking behavior. A decision-tree-based algorithm was proposed in [23] to decrease the peak demand in the residential distribution networks by coordinating the flexible EVs with vehicle-to-grid (V2G) capability with solar PV generation and battery energy storage. Fast response power electronic compensation at load side and feeder level, was used in [24] to control the voltage in the distribution network with variable PV generation and EV loads. A coordinated scheme for EV charging and PV generation was proposed in [25] to alleviate the flow imbalances among the phases in the distribution network. The coordinated operation of PVs and EVs in an unbalanced distribution network using energy storage was proposed in [26]. An online control approach was developed based on a rolling optimization framework to ensure the security of the distribution network by regulating the power output of PV generation units, EVs, and tap changer settings. In [27], differential evolution optimization was used to determine the PV and EV outputs that minimize the power loss and improve the voltage profile in an unbalanced distribution network. The hosting capacity assessment of combined PV-EV technology is carried out in [28] ignoring the uncertainty in EV interconnection.

While extensive research works exist on the operation of the distribution networks considering the uncertainties in the EV interconnections, EV owners' preferences, and solar PV generation; limited research efforts were made to determining the dispatch limits for PV generation in distribution networks considering the unbalanced EV interconnections and the corresponding uncertainties. Quantifying the dispatch limits for PV generation provides feasible operation regions that accommodate the PV generation in the distribution network. Such solutions would help the system operator to determine the upper and lower limits of the uncertainty sets associated with the PV generation that are required for solving the risk-based distribution network operation problems. In the bulk power network, quantifying do-not-exceed limits for renewable resources was proposed in [29]-[31]. In [29], a robust optimization problem was formulated to determine the dispatchability limits for a renewable resource. In [30] a datadriven algorithm was presented that aims to maximize the utilization of variable renewable generation by determining the do-not-exceed limits of this resource considering the operating points of the dispatchable resources. In the previous work [32], the dispatch limits of PV generation in the distribution network considering the uncertainty in EV interconnection were addressed using scenarios. This research is extended in this paper by capturing the worst-case realization of the maximum and minimum power and energy capacity, the available energy at arrival and departure times, and the arrival and departure times of EV clusters. Furthermore, the formulated problem is extended to a large-scale network in this paper.

C. Key contributions and organization of the paper The contributions of this paper are as follows:

- A mathematical formulation is proposed to quantify the dispatch limits of the PV generation on each phase considering the unbalanced operation of the distribution network.
- The proposed formulation addresses the worst-case realization of a) the arrival and departure times for EVs,
 b) the available energy at arrival and departure times, c) the maximum and minimum available energy and power for EVs, to quantify the dispatch limits of PV generation in the distribution network.
- The uncertainties associated with the maximum PV generation and demand are captured in the developed formulation using scenarios.

The rest of the paper is organized as follows: section II presents the problem formulation, in which the detailed descriptions of the objective function and constraints are presented. The robust optimization solution methodology is presented in section III. The numerical results are discussed in section IV. In this section, to evaluate the effectiveness of the proposed approach for small-scale and large-scale distribution networks, the modified IEEE 34-bus and IEEE 123-bus three-phase distribution systems are considered. Finally, the conclusion is presented in section V.

II. PROBLEM FORMULATION

The proposed problem formulation addresses the uncertainty in the arrival and departure times, the charging and discharging power capacity, the maximum and minimum storage capacity, and the available energy at arrival and

departure times for the EVs. The uncertainties in the forecasted maximum solar PV generation and electricity demand are captured in scenarios.

The problem formulation is shown in (1)-(60). The objective of this problem is shown in (1). The first term in the objective function aims to maximize the difference between the lower and upper dispatch limits of the PV generation units while ensuring that the PV outputs are within these limits. As shown in the second term of the objective function, the feasibility of the dispatched PV generation is ensured by minimizing the mismatch in nodal power balance with the worst-case realization of the uncertain variables. Minimizing the binary variable $V_{v,t}^{\phi,m}$ maintains the PV generation within the lower and upper dispatch limits. The next term is the normalized difference between the upper and lower dispatch limits of PV generation. In the second part of the objective function, vector $\boldsymbol{\nu}_{e,t}^{\phi,m}$ is a vector composed of the binary variables associated with the uncertainties in EVs (i.e. $\delta_{e,t}^{\phi,m} \in \boldsymbol{\nu}_{e,t}^{\phi,m}, \gamma_{e,t}^{\phi,m} \in \boldsymbol{\nu}_{e,t}^{\phi,m}, \beta_{e,t}^{\phi,m,arv} \in \boldsymbol{\nu}_{e,t}^{\phi,m}, \beta_{e,t}^{\phi,m,dep} \in \boldsymbol{\nu}_{e,t}^{\phi,m}, \mu_{e,t}^{\phi,m,dep} \in \boldsymbol{\nu}_{e,t}^{\phi,m}, \mu_{e,t}^{\phi,m,dep} \in \boldsymbol{\nu}_{e,t}^{\phi,m}$ and $\boldsymbol{\tau}_{e}^{\phi,m,dep} \in \boldsymbol{\nu}_{e,t}^{\phi,m}$.

The real and reactive power balances at each node of the distribution network are enforced by (2) and (3) respectively. The distribution branch power flow is formulated by (4), (5) as presented in [33]. Here, $PL_{l,t}^{\phi,m} \in PL_t^m$, $QL_{l,t}^{\phi,m} \in QL_t^m$, $U_{b,t}^{\phi,m} \in U_{b,t}^m$ and $\widetilde{R}_l, \widetilde{X}_l$ are obtained using [33]. The big-M method is used in (4) and (5) to address the availability of phases on the distribution branch. The circular constraint representing the complex power flow limit in a distribution branch is linearized in (6)-(11) using the technique presented in [34]. The real and reactive power outputs of a DG unit are bounded by (12) and (13) respectively. Constraints (14)-(19) enforce the limits on the real and reactive power supply of the distribution feeder. The acceptable power factor would limit the exchanged reactive power at the main distribution feeder as shown in (18) and (19). Constraints (20)-(21) show the limits on the real and reactive power outputs of the PV unit. As shown in (20) and (22), the PV generation is limited by the nominal capacity of the unit and the collected solar energy. The reactive power output of the PV unit is within the upper and lower capacity limits as shown in (21). The relationship between the lower and upper dispatch limits of PV generation is shown in (23). The upper PV dispatch limit is constrained by the nominal capacity of the PV generation unit as shown in (24). As enforced by (25) and (26), if $V_{v,t}^{\phi,m}$ is 0, the PV generation is within the dispatch limits and otherwise, it is out of the dispatch limits. Here, the worst-case realization of the PV generation is characterized by the lower or upper dispatch limits as shown in (27).

In the proposed formulation, EVs with similar characteristics are considered as a cluster. The uncertainties associated with the arrival and departure times i.e. $T_e^{\phi,m,arv}$ and $T_e^{\phi,m,dep}$, during which an EV cluster is connected to the distribution network are addressed by (28)-(44). Here, the arrival time is between a lower and an upper limit as shown in (28)-(29). The lower and upper limits are formulated using the forecasted arrival time and a difference between

the forecasted arrival time and the uncertain boundaries. Similarly, the departure time is between the lower and upper limits as shown in (30), (31). The relationship between the arrival time and the binary variable representing the arrival of the EV cluster $(IC_{e,t}^{A,\phi,m})$ is shown in (32), (33). As shown here, if $t \geq T_e^{\phi,m,arv}$ then $(IC_{e,t}^{A,\phi,m}=1)$ and otherwise $(IC_{e,t}^{A,\phi,m}=0)$. Similarly, the relationship between the departure time and the binary variable representing the departure of the EV cluster $(IC_{e,t}^{D,\phi,m})$ is shown in (34), (35). As shown here, if $t \geq T_e^{\phi,m,dep}$ then $(IC_{e,t}^{D,\phi,m}=0)$ and otherwise, $(IC_{e,t}^{D,\phi,m}=1)$. Here, $c_t^{\phi,m}$ is an auxiliary variable that accounts for the time index, and $T_e^{\phi,m,arv} \cdot IC_{e,t}^{A,\phi,m}$ is a nonlinear term that is further linearized using McCormick envelopes [35]. A similar technique is used to handle the nonlinear terms in (33)-(35). The interconnection state of an EV cluster is determined using (38)-(40). Here, $IC_{e,t}^{\phi,m}=1$ if the vehicle cluster e arrives at the charging station $(IC_{e,t}^{A,\phi,m}=1)$, and does not leave the charging station i.e. $(IC_{e,t}^{\widetilde{D},\phi,m}=1)$. The arriving and departing states of an EV cluster are determined by (41) and (42). Here, if an EV cluster leaves the charging station then $ID_{e,t}^{\phi,m}=1$, and when an EV cluster arrives at the charging station $IA_{e,t}^{\phi,m}=1$. The budgets of uncertainty for arrival and departure times are enforced by (43) and (44) respectively.

$$\min_{\substack{u_{v,t}^{\phi,m}, v_{v,t}^{\phi,m}, V_{v,t}^{\phi,m} = \sum \\ \sigma_{v,t}^{\phi,m}, \nu_{e,t}^{\phi,m} s_{(.)}^{(.)}} \sum_{m} \sum_{v} \sum_{\phi} \sum_{t} (V_{v,t}^{\phi,m} - (u_{v,t}^{\phi,m} - l_{v,t}^{\phi,m}) / P_{v}^{\phi,max}) \\
+ \max_{\substack{\sigma_{v,t}^{\phi,m}, \nu_{e,t}^{\phi,m} \\ s_{(.)}}} \min_{m} \sum_{b} \sum_{b} \sum_{t} (s_{b,t}^{1,\phi,m} + s_{b,t}^{2,\phi,m} + s_{b,t}^{3,\phi,m} + s_{b,t}^{4,\phi,m})$$
(1)

s.t

$$\sum_{l} AL_{l,b}PL_{l,t}^{\phi,m} + \sum_{i} AI_{i,b}P_{i,t}^{\phi,m} + \sum_{v} AV_{v,b}P_{v,t}^{\phi,m} + \sum_{e} AE_{e,b}(P_{e,t}^{\phi,m,dc} - P_{e,t}^{\phi,m,ch}) + \sum_{n} AN_{n,b}P_{n,t}^{\phi,m} + s_{b,t}^{1,\phi,m} - s_{b,t}^{2,\phi,m} = \sum_{d} AD_{d,b}P_{d,t}^{\phi,m}$$
 (2)

$$\sum_{l} AL_{l,b}QL_{l,t}^{\phi,m} + \sum_{i} AI_{i,b}Q_{i,t}^{\phi,m} + \sum_{v} AV_{v,b}Q_{v,t}^{\phi,m} + \sum_{e} AE_{e,b}Q_{e,t}^{\phi,m} + \sum_{n} AN_{n,b}Q_{n,t}^{\phi,m} + s_{b,t}^{3,\phi,m} - s_{b,t}^{4,\phi,m}$$

$$= \sum_{d} AD_{d,b}Q_{d,t}^{\phi,m} \quad (3)$$

$$AL_{l,b} \cdot \boldsymbol{U}_{b,t}^{m} + 2(\widetilde{\boldsymbol{R}}_{l} \cdot \boldsymbol{P} \boldsymbol{L}_{l,t}^{m} + \widetilde{\boldsymbol{X}}_{l} \cdot \boldsymbol{Q} \boldsymbol{L}_{l,t}^{m}) \leq M \cdot (1 - \boldsymbol{p}_{l}) \ \, (4)$$

$$AL_{l,b} \cdot \boldsymbol{U}_{b,t}^{m} + 2(\widetilde{\boldsymbol{R}}_{l} \cdot \boldsymbol{P} \boldsymbol{L}_{l,t}^{m} + \widetilde{\boldsymbol{X}}_{l} \cdot \boldsymbol{Q} \boldsymbol{L}_{l,t}^{m}) \ge -M \cdot (1 - \boldsymbol{p}_{l}) \quad (5)$$

$$-p_l^{\phi} \cdot SL_l^{\phi,max} \le PL_{l,t}^{\phi,m} \le p_l^{\phi} \cdot SL_l^{\phi,max} \tag{6}$$

$$-p_l^{\phi} \cdot SL_l^{\phi,max} \le QL_{l,t}^{\phi,m} \le p_l^{\phi} \cdot SL_l^{\phi,max} \tag{7}$$

$$-\sqrt{2} \cdot p_l^{\phi} \cdot SL_l^{\phi,max} \le PL_{l,t}^{\phi,m} + QL_{l,t}^{\phi,m} \tag{8}$$

$$PL_{l,t}^{\phi,m} + QL_{l,t}^{\phi,m} \le \sqrt{2} \cdot p_l^{\phi} \cdot SL_l^{\phi,max} \tag{9}$$

$$-\sqrt{2} \cdot p_l^{\phi} \cdot SL_l^{\phi,max} \le PL_{l,t}^{\phi,m} - QL_{l,t}^{\phi,m} \tag{10}$$

$$PL_{l,t}^{\phi,m} - QL_{l,t}^{\phi,m} \le \sqrt{2} \cdot p_l^{\phi} \cdot SL_l^{\phi,max} \tag{11}$$

$$0 \le P_{i,t}^{\phi,m} \le P_i^{\phi,max} \tag{12}$$

$$-Q_i^{\phi,max} \le Q_{i,t}^{\phi,m} \le Q_i^{\phi,max} \tag{13}$$

$$-S_n^{\phi,max} \le P_{n,t}^{\phi,m} \le S_n^{\phi,max} \tag{14}$$

$$-S_n^{\phi,max} \le Q_{n,t}^{\phi,m} \le S_n^{\phi,max} \tag{15}$$

$$-\sqrt{2} \cdot S_{n}^{\phi, max} \le P_{n,t}^{\phi, m} + Q_{n,t}^{\phi, m} \le \sqrt{2} \cdot S_{n}^{\phi, max} \tag{16}$$

$$-\sqrt{2} \cdot S_n^{\phi,max} \le P_{n,t}^{\phi,m} - Q_{n,t}^{\phi,m} \le \sqrt{2} \cdot S_n^{\phi,max} \tag{17}$$

$$Q_{n,t}^{\phi,m} \le \tan\left(\cos^{-1}PF_n\right) \cdot P_{n,t}^{\phi,m} \tag{18}$$

$$Q_{n,t}^{\phi,m} \ge -\tan\left(\cos^{-1}PF_n\right) \cdot P_{n,t}^{\phi,m} \tag{19}$$

$$0 \le P_{v,t}^{\phi,m} \le P_v^{\phi,max} \tag{20}$$

$$-Q_v^{\phi,max} \le Q_{v,t}^{\phi,m} \le Q_v^{\phi,max} \tag{21}$$

$$P_{v,t}^{\phi,m} \le A_v^{\phi}.IR_{v,t}^m \tag{22}$$

$$0 \le l_{v,t}^{\phi,m} \le u_{v,t}^{\phi,m} \tag{23}$$

$$u_{v,t}^{\phi,m} \le P_v^{\phi,max} \tag{24}$$

$$\left(P_{v}^{\phi,max} - A_{v}^{\phi}.IR_{v,t}^{m}\right).V_{v,t}^{\phi,m} - l_{v,t}^{\phi,m} \ge -A_{v}^{\phi}.IR_{v,t}^{m} \quad (25)$$

$$A_v^{\phi}.IR_{v,t}^m \cdot V_{v,t}^{\phi,m} + u_{v,t}^{\phi,m} \le A_v^{\phi} \cdot IR_{v,t}^m$$
 (26)

$$P_{v,t}^{\phi,m} = l_{v,t}^{\phi,m} + \left(u_{v,t}^{\phi,m} - l_{v,t}^{\phi,m}\right) . \sigma_{v,t}^{\phi,m} \tag{27}$$

$$T_{e}^{\phi,m,arv} \geq \hat{T}_{e}^{\phi,arv} - \tau_{e}^{\phi,m,arv} \cdot \widetilde{T}_{e}^{\phi,arv,min} \tag{28}$$

$$T_e^{\phi,m,arv} \le \hat{T}_e^{\phi,arv} + \tau_e^{\phi,m,arv} \cdot \tilde{T}_e^{\phi,arv,max}$$
 (29)

$$T_e^{\phi,m,dep} \ge \hat{T}_e^{\phi,dep} - \tau_e^{\phi,m,dep} \cdot \tilde{T}_e^{\phi,dep,min}$$
 (30)

$$T_e^{\phi,m,dep} \leq \hat{T}_e^{\phi,dep} + \tau_e^{\phi,m,dep} \cdot \tilde{T}_e^{\phi,dep,max} \tag{31} \label{eq:31}$$

$$c_t^{\phi,m} - T_e^{\phi,m,arv} \cdot IC_{e,t}^{A,\phi,m} \ge 0 \tag{32}$$

$$c_t^{\phi,m} - \left(NT - T_e^{\phi,m,arv}\right) \cdot IC_{e,t}^{A,\phi,m} \le T_e^{\phi,m,arv} \tag{33}$$

$$c_t^{\phi,m} + \left(NT - T_e^{\phi,m,dep}\right) \cdot IC_{e,t}^{D,\phi,m} \le NT$$
 (34)

$$c_t^{\phi,m} + T_e^{\phi,m,dep} \cdot IC_{e,t}^{D,\phi,m} \ge T_e^{\phi,m,dep} \tag{35} \label{eq:35}$$

$$c_t^{\phi,m} \le NT \tag{36}$$

$$c_t^{\phi,m} - c_{t-1}^{\phi,m} = 1 (37)$$

$$IC_{e,t}^{\phi,m} \le IC_{e,t}^{A,\phi,m} \tag{38}$$

$$IC_{e,t}^{\phi,m} \le IC_{e,t}^{D,\phi,m} \tag{39}$$

$$IC_{e,t}^{\phi,m} \ge IC_{e,t}^{A,\phi,m} + IC_{e,t}^{D,\phi,m} - 1$$
 (40)

$$IC_{e,t-1}^{\phi,m} - IC_{e,t}^{\phi,m} = ID_{e,t-1}^{\phi,m} - IA_{e,t}^{\phi,m}$$
 (41)

$$ID_{e,t-1}^{\phi,m} + IA_{e,t}^{\phi,m} \le 1$$
 (42)

$$\sum_{e} \tau_e^{\phi, m, arv} \le \Lambda^{\phi, arv} \tag{43}$$

$$\sum_{e} \tau_e^{\phi, m, dep} \le \Lambda^{\phi, dep} \tag{44}$$

$$\hat{E}_{e}^{\phi,min} + \delta_{e,t}^{\phi,m} \cdot \widetilde{E}_{e}^{\phi,min} - M(1 - IC_{e,t}^{\phi,m}) \le E_{e,t}^{\phi,m} \quad (45)$$

$$E_{e,t}^{\phi,m} \le \hat{E}_e^{\phi,max} + \gamma_{e,t}^{\phi,m} \cdot \widetilde{E}_e^{\phi,max} + M(1 - IC_{e,t}^{\phi,m})$$
 (46)

$$E_{e,t}^{\phi,m} \le \left(\hat{l}_e^{\phi,arv} + \beta_{e,t}^{\phi,m,arv} \cdot \tilde{l}_e^{\phi,arv}\right) \cdot \left(\hat{E}_e^{\phi,min} + \delta_{e,t}^{\phi,m} \cdot \widetilde{E}_e^{\phi,min}\right) + M \cdot \left(1 - IA_{e,t}^{\phi,m}\right)$$
(47)

$$E_{e,t}^{\phi,m} \ge \left(\hat{l}_e^{\phi,arv} + \beta_{e,t}^{\phi,m,arv} \cdot \tilde{l}_e^{\phi,arv}\right) \cdot \left(\hat{E}_e^{\phi,min} + \delta_{e,t}^{\phi,m} \cdot \tilde{E}_e^{\phi,min}\right) - M \cdot \left(1 - IA_{e,t}^{\phi,m}\right)$$
(48)

$$E_{e,t}^{\phi,m} \le \left(\hat{l}_e^{\phi,dep} + \beta_{e,t}^{\phi,m,dep} \cdot \tilde{l}_e^{\phi,dep}\right) \cdot \left(\hat{E}_e^{\phi,max} + \gamma_{e,t}^{\phi,m} \cdot \tilde{E}_e^{\phi,max}\right) + M \cdot \left(1 - ID_{e,t}^{\phi,m}\right)$$
(49)

$$E_{e,t}^{\phi,m} \ge \left(\hat{l}_e^{\phi,dep} + \beta_{e,t}^{\phi,m,dep} \cdot \tilde{l}_e^{\phi,dep}\right) \cdot \left(\hat{E}_e^{\phi,max} + \gamma_{e,t}^{\phi,m} \cdot \tilde{E}_e^{\phi,max}\right) - M \cdot \left(1 - ID_{e,t}^{\phi,m}\right)$$
(50)

$$0 \leq P_{e,t}^{\phi,m,ch} \leq IC_{e,t}^{\phi,m} \cdot \left(\hat{P}_{e}^{\phi,ch,max} + \mu_{e,t}^{\phi,m,ch} \cdot \widetilde{P}_{e}^{\phi,ch,max}\right)$$

$$0 \leq P_{e,t}^{\phi,m,dc} \leq IC_{e,t}^{\phi,m} \cdot \left(\hat{P}_{e}^{\phi,dc,max} + \mu_{e,t}^{\phi,m,dc} \cdot \widetilde{P}_{e}^{\phi,dc,max}\right)$$

$$(51)$$

$$E_{e,t}^{\phi,m} - E_{e,t-1}^{\phi,m} - \eta_{ch}^{e} P_{e,t}^{\phi,m,ch} + P_{e,t}^{\phi,m,dc} / \eta_{dc}^{e} \le M \cdot \left(1 - IC_{e,t}^{\phi,m}\right) \quad (53)$$

$$E_{e,t}^{\phi,m} - E_{e,t-1}^{\phi,m} - \eta_{ch}^{e} P_{e,t}^{\phi,m,ch} + P_{e,t}^{\phi,m,dc} / \eta_{dc}^{e} \ge -M \cdot \left(1 - IC_{e,t}^{\phi,m}\right) \quad (54)$$

$$\sum_{e} \sum_{t} \delta_{e,t}^{\phi,m} \le \Gamma^{\phi,E_{min}} \tag{55}$$

$$\sum_{e} \sum_{t} \gamma_{e,t}^{\phi,m} \le \Gamma^{\phi,E_{max}} \tag{56}$$

$$\sum_{e} \sum_{t} \beta_{e,t}^{\phi,m,arv} \le \Gamma^{\phi,arv} \tag{57}$$

$$\sum_{e} \sum_{t} \beta_{e,t}^{\phi,m,dep} \le \Gamma^{\phi,dep} \tag{58}$$

$$\sum_{e} \sum_{t} \mu_{e,t}^{\phi,m,ch} \le \Gamma^{\phi,ch} \tag{59}$$

$$\sum_{e} \sum_{t} \mu_{e,t}^{\phi,m,dc} \le \Gamma^{\phi,dc} \tag{60}$$

Once, an EV cluster e is connected to the grid, constraints (45) and (46) enforce the limits for the available energy in its batteries. The available energy at arrival and departure times is enforced by (47)-(50) using the big-M method. The available energy at arrival and departure times is uncertain and defined as a portion of the maximum and minimum capacity

of the EV cluster batteries. In (47), the first term on the righthand side represents the uncertainty in the state of charge in terms of the minimum battery capacity of EVs and the second term represents the uncertainty in the minimum capacity of EV batteries connected to the distribution network. Similarly, in (49), the first term on the right-hand side represents the uncertainty in the state of charge in terms of the maximum battery capacity of EVs while the second term represents the uncertainty in the maximum capacity of EV batteries connected to the distribution network. The power dispatch for an EV cluster is limited by (51), (52). The charging and discharging power of an EV cluster before the arrival time and after the departure time is zero. The hourly stored energy in an EV cluster is determined by its charging and discharging power dispatch as shown by (53) and (54). The budget of uncertainty for the minimum and maximum battery capacity of EV clusters, the available energy at arrival and departure times, and the maximum charging and discharging power of EV clusters are enforced by (55)-(60) respectively.

III. SOLUTION METHODOLOGY

The proposed solution methodology is based on the column and constraint generation (C&CG) technique. The steps taken to solve this problem are as follows:

- 1) Step 1 Initialization: Initialize the upper and lower bounds and the iteration counter k as follows: $LB=-\infty$, $UB=\infty$, k=0
- 2) Step 2 Solve the master problem: Solve the problem (61)-(67) and update the lower bound.

$$\min_{\mathbf{x}} \ \mathbf{c}^{\top} \mathbf{x} + \eta \tag{61}$$

s.t.

$$Ax < d \tag{62}$$

$$\eta \ge \boldsymbol{b}^{\top} \boldsymbol{s}^{\omega} \tag{63}$$

$$Dy^{\omega} \le g; \forall \omega \le k$$
 (64)

$$Hy^{\omega} + s^{\omega} = f; \forall \omega \le k \tag{65}$$

$$(E + M\sigma_{\omega}^*)x + Gy^{\omega} = h; \forall \omega \le k$$
 (66)

$$N\nu_{\omega}^* + Fy^{\omega} \le q; \forall \omega \le k$$
 (67)

Here, \boldsymbol{x} represents the vector of first-stage decision variables i.e. $\begin{bmatrix} l_{v,t}^{\phi,m}, u_{v,t}^{\phi,m}, V_{v,t}^{\phi,m} \end{bmatrix}$, and \boldsymbol{y} represents the second-stage recourse decision variables i.e. $P_{v,t}^{\phi,m}, P_{e,t}^{\phi,m,ch}, P_{e,t}^{\phi,m,dc}, P_{n,t}^{\phi,m}, P_{i,t}^{\phi,m}, Q_{v,t}^{\phi,m}, Q_{n,t}^{\phi,m}, Q_{i,t}^{\phi,m}$, and the state variables $PL_{l,t}^{\phi,m}, QL_{l,t}^{\phi,m}$ and $U_{b,t}^{m}$. The constraint (62) represents (23)-(26); constraint (64) represents the set of constraints (4)-(22). The constraint (65) represents (2) and (3). Constraint (66) represents (27) and constraint (67) represents (45)-(60). The lower bound is determined using (68).

$$LB = \sum_{m} \sum_{v} \sum_{\phi} \sum_{t} \left[\hat{V}_{v,t}^{\phi,m} - (\hat{u}_{v,t}^{\phi,m} - \hat{l}_{v,t}^{\phi,m}) / P_{v}^{\phi,max} \right]$$

3) Step 3 - Solve subproblem: Solve the subproblem (69)-(75) and update the upper bound using (82). Here, (74) represents

(28)-(40) and (42)-(44). The constraint (75) represents (41). To solve the subproblem, the problem (69)-(75) is transformed into (76)-(81) using the duality theory. The nonlinear terms $\sigma^{\top}\pi_3$ and $\nu^{\top}\pi_4$ are linearized using McCormick envelopes [35].

$$\max_{\boldsymbol{\sigma}_{v,t}^{\phi,m}, \boldsymbol{\nu}_{e,t}^{\phi,m}} \min_{\boldsymbol{s}} \boldsymbol{b}^{\top} \boldsymbol{s}$$
 (69)

s.t.

$$Dy \le g \qquad : \pi_1 \tag{70}$$

$$Hy + s = f \qquad : \pi_2 \tag{71}$$

$$Gy = h - (E + M\sigma)x^* : \pi_3$$
 (72)

$$Fy \le q - N\nu \qquad : \pi_4 \tag{73}$$

$$Wz < R \tag{74}$$

$$Qz = J \tag{75}$$

$$\Theta = \max_{\boldsymbol{\sigma}_{v,t}^{\phi,m},\boldsymbol{\nu}_{e,t}^{\phi,m},s} \boldsymbol{g}^{\top}\boldsymbol{\pi}_{1} + \boldsymbol{f}^{\top}\boldsymbol{\pi}_{2} + \left[\boldsymbol{h} - (\boldsymbol{E} + \boldsymbol{M}\boldsymbol{\sigma})\boldsymbol{x}^{*}\right]^{\top}\boldsymbol{\pi}_{3} +$$

$$(\boldsymbol{q} - \boldsymbol{N} \boldsymbol{\nu})^{\top} \boldsymbol{\pi}_4 \quad (76)$$

$$\boldsymbol{D}^{\top}\boldsymbol{\pi}_{1} + \boldsymbol{H}^{\top}\boldsymbol{\pi}_{2} + \boldsymbol{G}^{\top}\boldsymbol{\pi}_{3} + \boldsymbol{F}^{\top}\boldsymbol{\pi}_{4} \leq 0$$
 (77)

$$\pi_2 \le b, \quad \pi_3 \quad free$$
 (78)

$$\pi_1, \ \pi_4 < 0$$
 (79)

$$Wz \le R$$
 (80)

$$Qz = J \tag{81}$$

$$UB = min\{UB, \sum_{m} \sum_{v} \sum_{\phi} \sum_{t} (\hat{V}_{v,t}^{\phi,m} - \frac{\hat{u}_{v,t}^{\phi,m} - \hat{l}_{v,t}^{\phi,m}}{p_{v}^{\phi,max}}) + \Theta^{*(k+1)}\}$$
(82)

4) Step 4 - Checking the convergence criterion: If $UB-LB \le \varepsilon$, then terminate the algorithm, otherwise go to Step 5.
5) Step 5 - Generate columns and constraints: Add constraints (63)-(67) to the master problem and go to Step 2. Algorithm 1 is the proposed algorithm to determine the PV dispatch limits in which K represents the maximum number of iterations.

IV. NUMERICAL RESULTS

Two test cases are considered in this section. The first test case uses the modified IEEE 34-bus system and the second test case presents the modified IEEE 123-bus system. The simulations are performed on a server with dual 14 Core Intel Xeon 2.6 GHz and 380 GB of memory. CPLEX 12.8 is used as the solver.

Algorithm 1 The proposed algorithm to quantify the PV dispatch limits

Initialization: $k=0, \ \varepsilon \leq 10^{-3}, \ LB=-\infty \ \text{and} \ UB=\infty$ **Repeat** for $m \in \mathcal{M}$

1: while $k \leq K$ do

2: Solve the master problem (61)-(67).

3: Update the LB as given in (68).

4: Solve the subproblem (76)-(81).

5: Update the UB as given in (82).

6: Check the convergence criteria:

7: **if** $(UB - LB \le \varepsilon)$ **then**

8: Stop

9: else

10: Generate column and constraints (63)-(67) and set k = k + 1.

11: **end if**

12: end while

A. Modified IEEE 34-bus system

The modified IEEE 34-bus distribution system is considered as a test case. The hourly peak demand and hourly PV outputs are shown in Fig. 1. One three-phase and three single-phase dispatchable DG units are installed as shown in Table I. Here, DG1 is a three-phase DG unit and DG2-DG4 are single-phase DG units connected to phases A, B, and C respectively. Three single-phase PV units, i.e. PV1, PV2, and PV3 are connected to phases A, B, and C respectively. The characteristics of the PV generation units are shown in Table II. Table III shows the characteristics of the EV clusters. Here, the interconnection of EV cluster 1 is three-phase; however, the EV clusters 2-4 are connected to phases A, B, and C respectively. The maximum charging power for each EV is 7.4 kW. The peak demand on phase A is $593.88 \ kW$, $349.86 \ kVar$, the peak demand on phase B is 572.32~kW and 337.12~kVar, and the peak demand on phase C is 567.42 kW and 336.14 kVar. Considering the driving range of 27.9 miles per day for each EV [36], and 30 kWh battery capacity, the forecasted stored energy at arrival time is 60% of the maximum capacity and the EV. The charging and discharging efficiency for the EV clusters are 90%. The following cases are considered:

Case 1 – PV dispatch limits with forecasted PV generation and demand.

Case 2 - PV dispatch limits with forecasted PV generation and demand, and the uncertainty in the EV interconnection.

Case 3 – PV dispatch limits with stochastic forecasted PV generation and demand, and the uncertainty in the EV interconnection.

TABLE I: Dispatchable DG Units' Characteristics

DG	Bus	P^{min}	P^{max}	Q^{min}	Q^{max}
		(kW)	(kW)	(kVAR)	(kVAR)
1	4	0	60	-30	30
2	6	0	50	-25	25
3	24	0	20	-15	15
4	16	0	20	-15	15

1) Case 1 - PV dispatch limits with forecasted PV generation and demand: In this case, the PV dispatch limits

TABLE II: PV Generation Units' Characteristics

PV	Bus	P^{min}	P^{max}	Q^{min}	Q^{max}
		(kW)	(kW)	(kVAR)	(kVAR)
1	17	0	150	-75	75
2	22	0	150	-75	75
3	30	0	150	-75	75

TABLE III: Characteristics of EV Units

EV	Number	Bus	P^{max}	E^{min}	E^{max}
cluster	of vehicles		(kW)	(kWh)	(kWh)
1	24	4	177.6	72	720
2	3	6	22.2	9	90
3	4	24	29.6	12	120
4	3	16	22.2	9	90

are procured without considering any EV interconnection to the distribution network. The forecasted values of the maximum PV generation and demand are used in this case. The PV dispatch limits on each phase are demonstrated in Fig. 2. At hours in which the lower limit of PV generation is greater than zero, the distribution feeder and DGs are incapable of supplying the demand, and therefore; the rest of the demand is supplied by the PV generation units. For example, on phase B at hour 11, the lower limit of the PV generation is $27.927 \ kW$. At this hour, the total real power demand is $566.480 \ kW$, and the dispatch of the main distribution feeder, DG1, and DG3, are $498.553 \ kW$, $20 \ kW$, and $20 \ kW$ respectively. Here, DGs and the distribution feeder reached their maximum capacity on this phase, and consequently, the rest of the load (i.e. $27.927 \ kW$) is supplied by the PV generation units.

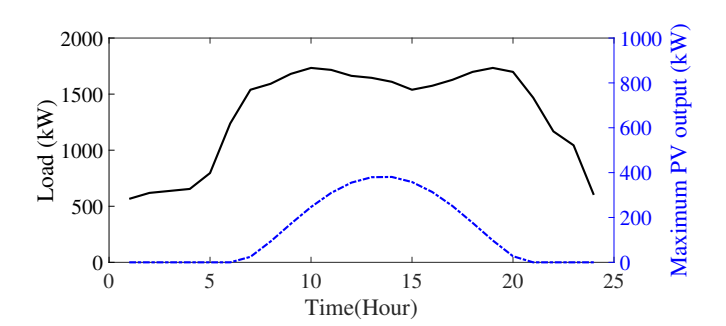


Fig. 1: Demand and maximum PV generation profiles

2) Case 2 – PV dispatch limits with forecasted PV generation and demand, and the uncertainty in the EV interconnection: In Case 2, the EV interconnection and the worst-case realization of the uncertain parameters in the EV clusters including the maximum and minimum EV battery capacities, the maximum charging and discharging power for EVs, the available energy at arrival and departure times, as well as the arrival and departure times are considered.

The uncertainty sets for maximum available energy are $[684,720] \, kWh$, $[81,90] \, kWh$, $[108,120] \, kWh$, and $[81,90] \, kWh$ for the first to fourth EV clusters, respectively. The uncertainty sets for the minimum available energy are $[72,144] \, kWh$, $[9,18] \, kWh$, $[12,24] \, kWh$, and $[9,18] \, kWh$ for the first to fourth EV clusters, respectively. The uncertainty sets for available energy at arrival time are $[396,468] \, kWh$, $[49.5,58.5] \, kWh$, $[66,78] \, kWh$, and $[49.5,58.5] \, kWh$ for

TABLE IV: Total Lower PV Dispatch Limits with the Budget of Uncertainty

Budget of Uncertainty [%]								Total lower dispatch limits on each phase (kWh)			
Scenario	$\Gamma^{\phi,E_{min}}$	$\Gamma^{\phi,E_{max}}$	$\Gamma^{\phi,arv}$	$\Gamma^{\phi,dep}$	$\Gamma^{\phi,ch}$	$\Gamma^{\phi,dc}$	Phase A	Phase B	Phase C	Iterations	
1 (Case 2)	100	100	100	100	100	100	245.630	345.487	268.537	7	
2	0	0	100	100	100	100	210.630	293.460	230.770	6	
3	0	0	0	0	100	100	179.130	257.460	197.770	4	
4	0	0	0	0	0	0	179.130	257.460	197.770	4	
-			Case 1				80.493	111.88	82.873	2	

TABLE V: Worst-Case Realization of Arrival and Departure Times for the IEEE 34-bus System

Arrival and departure times for EV clusters on buses 6, 24 and 16 [hour]												
Scenario	$T_1^{a,arv}$	$T_1^{a,dep}$	$T_1^{b,arv}$	$T_1^{b,dep}$	$T_1^{c,arv}$	$T_1^{c,dep}$	$T_2^{a,arv}$	$T_2^{a,dep}$	$T_3^{b,arv}$	$T_3^{b,arv}$	$T_4^{c,arv}$	$T_4^{c,dep}$
1 (Case 2)	10	17	10	17	10	17	10	17	10	15	8	15
2	8	15	8	17	8	17	10	15	10	15	10	17
3	10	17	10	17	10	17	10	15	8	17	8	15
4	10	17	10	17	10	17	10	17	10	15	8	15

TABLE VI: Total Lower Dispatch Limits of the PV Generation

			wer dispatcach phase (k						
Scenario	$\Lambda^{a,arv}$	$\Lambda^{a,dep}$	$\Lambda^{b,arv}$	Phase A	Phase B	Phase C			
5 (Case 2)	100	100	100	100	100	100	245.630	345.487	268.537
6	50	50	50	50	50	50	223.430	301.033	240.797
7	0	0	100	100	100	100	186.183	345.487	268.537
8	0	0	0	0	100	100	186.183	287.967	268.537
9	0	0	0	0	0	0	186.183	287.967	214.500

first to fourth EV clusters, respectively. The uncertainty sets for the available energy at departure time are [583.2,720] kWh, [72.9,90] kWh, [97.2,120] kWh, and [72.9,90] kWh for first to fourth EV clusters, respectively. The uncertainty sets for the maximum charging/discharging power dispatch are [177.6,213.2] kW, [22.2,26.64] kW, [29.6,35.52] kW, and [22.2,26.64] kW for the first to fourth EV clusters, respectively. Finally, the uncertainty sets for arrival and departure times are $T_e^{\Phi,arv} \in [8,10]$ and $T_e^{\Phi,dep} \in [15,17]$, respectively.

Fig. 2 demonstrates the dispatch limits for the PV generation units in this case. As shown in this figure, the lower PV dispatch limits on all phases at all hours are either equal or greater than those in Case 1. The solution algorithm converges after 7 iterations in this case. Considering the interconnection of EVs to the distribution network, the following observations were made:

a) The impact of V2G on the dispatch limits of PV generation To investigate the impacts of V2G on the PV dispatch limits, it is assumed that the EV clusters are unable to discharge and inject power back to the grid (non-V2G mode). Fig. 2 shows the dispatch limits for PV generation with and without V2G mode. Here, the lower dispatch limits for PV generation at all hours are either higher than or equal to the lower dispatch limits in Case 1, because the EVs are incapable of injecting power to the grid. As shown in Fig. 2c, on phase C at hours 12, 13, and 14, the lower PV dispatch limits are increased from 0 kW in Case 1 to 33.773 kW, 86.597 kW and 54.767 kW respectively.

b) The impact of the budget of uncertainty

The budget of uncertainty is defined as the maximum number

of changes allowed for the uncertain parameters within the defined uncertainty sets. Such changes are represented by the changes in the binary variables $\delta_{e,t}^{\phi,m}$, $\gamma_{e,t}^{\phi,m}$, $\beta_{e,t}^{\phi,m,arv}$, $\mu_{e,t}^{\phi,m,dep}$, $\mu_{e,t}^{\phi,m,dep}$, $\mu_{e,t}^{\phi,m,de}$, $\mu_{e,t}^{\phi,m,de}$, $\tau_{e}^{\phi,m,arv}$, $\tau_{e}^{\phi,m,dep}$, during the operation horizon. For instance, for maximum EV clusters' energy capacity, $\Gamma^{\phi,E_{max}} = 0$ means that the budget of uncertainty is 0%, while for the EV clusters on each phase in 24 hours, $\Gamma^{\phi,E_{max}} = 48$ indicates that the budget of uncertainty is 100%. To evaluate the impact of the budget of uncertainty on the PV dispatch limits, multiple scenarios shown in Table IV, are considered. This table shows the total lower dispatch limits for the PV generation in the distribution network by limiting the budget of uncertainty for 1) the minimum and maximum EV energy capacity, 2) minimum and maximum charging and discharging power, and 3) available energy at arrival and departure times. In these scenarios, the budgets of uncertainty for the arrival and departure times are 100%. Table V shows the worst-case realization of the arrival and departure times for the EV clusters on phases A, B, and C in the scenarios presented in Table IV. Fig. 3 demonstrates the PV dispatch limits on phases A, B, and C in these scenarios.

The impacts of the budgets of uncertainty $(\Lambda^{\phi,arv})$ and $\Lambda^{\phi,dep}$ on the total lower PV dispatch limits are shown using the scenarios in Table VI. Here, the budgets of uncertainty for the maximum and minimum energy and power capacities of EVs as well as the energy at arrival and departure times are 100%. As shown in this table, when the budgets of uncertainty for arrival and departure times decrease from 100% to 50%, the total lower dispatch limits on phases A, B, and C decrease by 9.04%, 12.87%, and 10.33% respectively. It is worth noting that 100% budget of uncertainty for the arrival and departure times means, $\Lambda^{\phi,arv}=2$ and $\Lambda^{\phi,dep}=2$ and 0% budget of

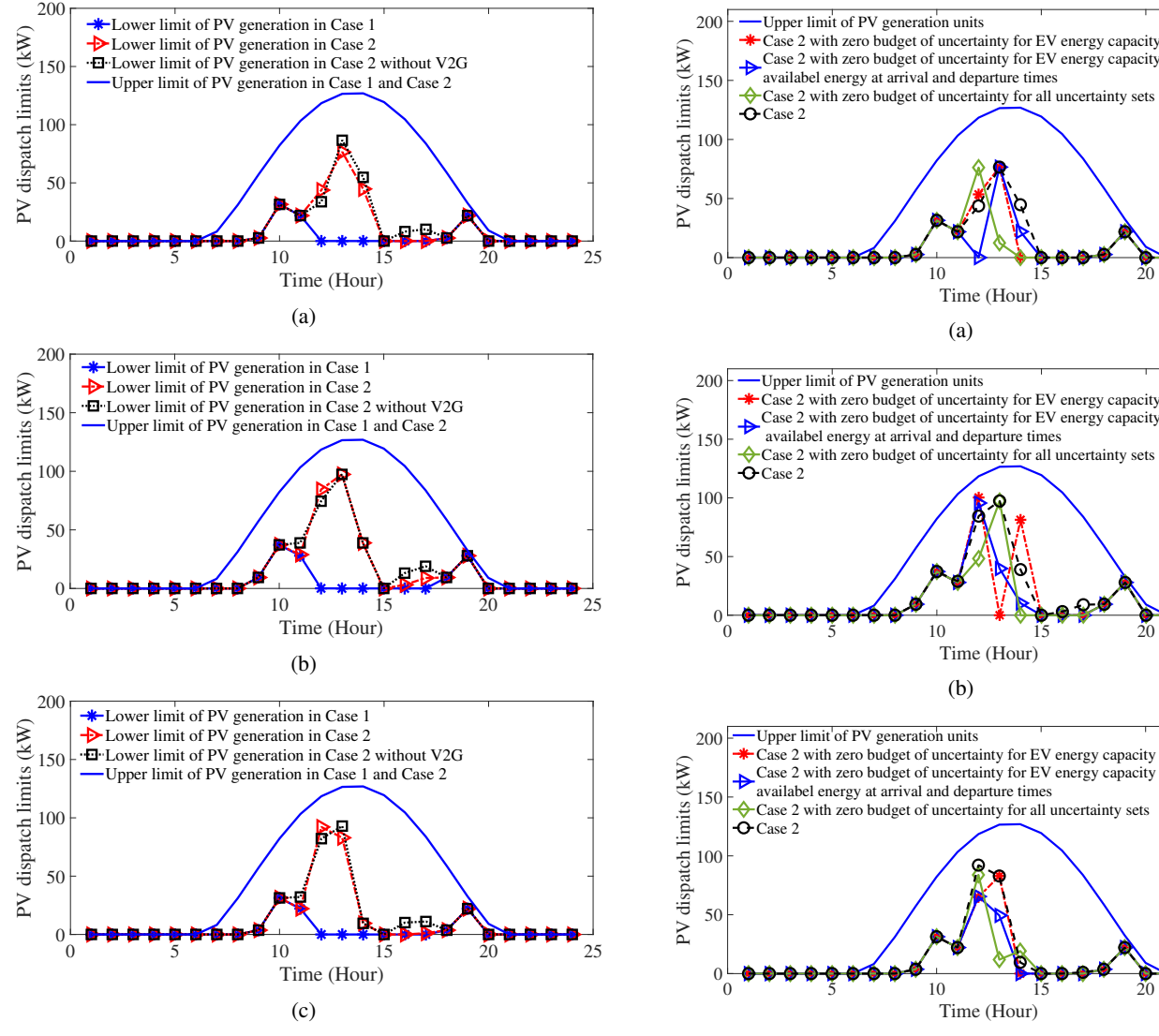


Fig. 2: The total PV dispatch limits for (a) phase A, (b) phase B and (c) phase C in Case 1 and Case 2 with and without V2G.

uncertainty means $\Lambda^{\phi,arv} = 0$ and $\Lambda^{\phi,dep} = 0$.

As it is shown in Fig. 3 and Table IV, once the budget of uncertainty is 100% for all the uncertain variables (Case 2), the total lower PV dispatch limit reaches its maximum value. In Table IV, the highest total lower PV dispatch limits are 245.630 kWh, 345.487 kWh, and 268.537 kWh on phases A, B, and C respectively. Moreover, once the budgets of uncertainty for the EVs' energy and power capacity, and the available energies at arrival and departure times, are zero the total lower PV dispatch limits for the PV generation on phases A, B, and C reach the lowest values of $179.130 \ kWh$, 257.460 kWh, and 197.770 kWh respectively. Table IV shows the number of iterations in which the proposed solution algorithm converged.

3) Case 3 – PV dispatch limits with stochastic forecasted PV generation and demand, and the uncertainty in the EV

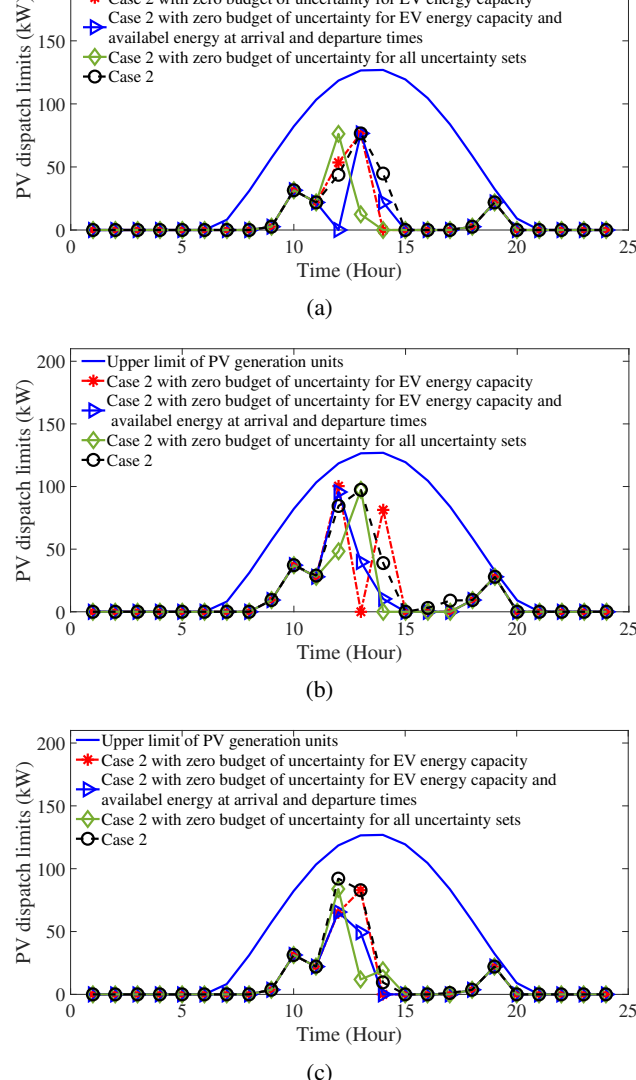


Fig. 3: The total PV dispatch limits for (a) phase A, (b) phase B and (c) phase C in Case 2 with the budget of uncertainty.

TABLE VII: Lower PV Dispatch Limits Considering the Uncertainty in the Forecasted PV Generation and Demand

Scenario	Phase A	Phase B	Phase C
S1	122.714	196.331	108.155
S2	127.682	201.118	114.754
S3	257.925	337.235	277.360
S4	319.060	394.124	343.449
S5	415.159	482.840	450.023
Expected Value	238.142	311.915	249.399
Case 2	245.630	345.487	268.537

interconnection: In this case, the forecast errors in demand and maximum PV generation are captured by generating 100 scenarios. The Gaussian probability distribution is used to represent the forecast error of the maximum PV generation. The mean value of the probability distribution is the forecasted PV generation in Cases 1 and 2, and the standard deviation is 0.0166 of the mean value. The hourly total upper and lower

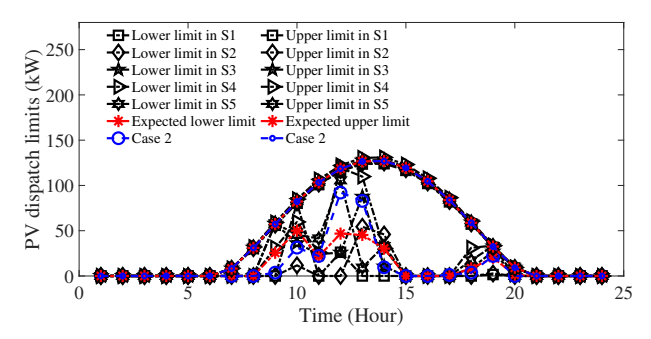


Fig. 4: The PV dispatch limits for stochastic PV generation and demand in 5 scenarios and the expected value for 100 scenarios on phase C.

TABLE VIII: Characteristics of PV Generation Units in the IEEE 123-Bus System

PV	Bus	P^{min}	P^{max}	Q^{min}	Q^{max}
1	1	0	400	-200	200
2	13	0	400	-200	200
3	18	0	400	-200	200
4	25	0	400	-200	200
5	40	0	200	-100	100
6	48	0	200	-100	100
7	60	0	200	-100	100
8	70	0	400	-200	200
9	81	0	200	-100	100
10	87	0	400	-200	200
11	101	0	400	-200	200
12	115	0	400	-200	200

dispatch limits of PV generation on phase C in 5 scenarios (S1-S5) and the expected upper and lower limits for 100 scenarios are shown in Fig. 4. Furthermore, Table VII shows the dayahead total lower dispatch limits for 5 scenarios and the expected value for 100 scenarios for all phases. The expected upper and lower dispatch limits of PV generation for 100 scenarios are compared to those presented in Case 2. As shown in Table VII, the expected total lower PV dispatch limits are smaller than those in Case 2.

B. Modified IEEE 123-Bus System

Here, the real and reactive peak demands on phase A are $1420\ kW$ and $775\ kVar$; on phase B are $915\ kW$, $515\ kVar$; and on phase C are $1155\ kW$ and $635\ kVar$, respectively. As shown in Table VIII, $12\ solar\ PV$ generation units are installed and the characteristics of the DG units are shown in Table IX. Here, DG4 and DG5 are single-phase DGs connected to phase A, and other DG units are three-phase resources. The characteristics of 6 EV clusters are shown in Table X where EV clusters 1 and 4 are on phase A, EV clusters 2 and 5 are on phase B, and EV clusters 3 and 6 are on phase C. The upper and lower limits of PV generation are evaluated in the following cases:

Case 1 – PV dispatch limits with forecasted PV generation and demand

Case 2 - PV dispatch limits with forecasted PV generation and demand, and the uncertainty in the EV interconnection

TABLE IX: Characteristics of DG Units in the IEEE 123-Bus System

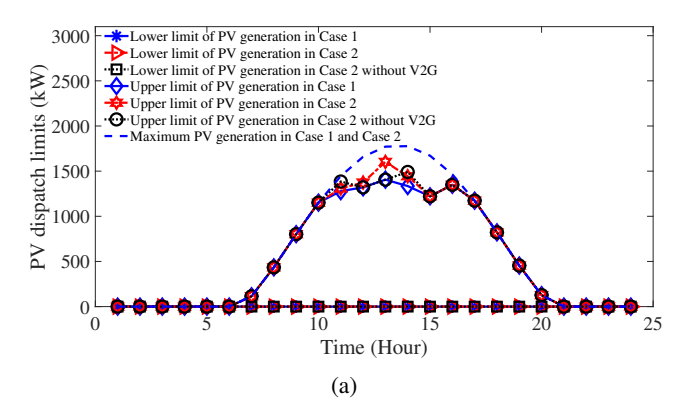
DG	Bus	P^{min}	P^{max}	Q^{min}	Q^{max}
1	29	0	100	-60	60
2	8	0	100	-60	60
3	44	0	100	-60	60
4	111	0	150	-75	75
5	122	0	50	-25	25

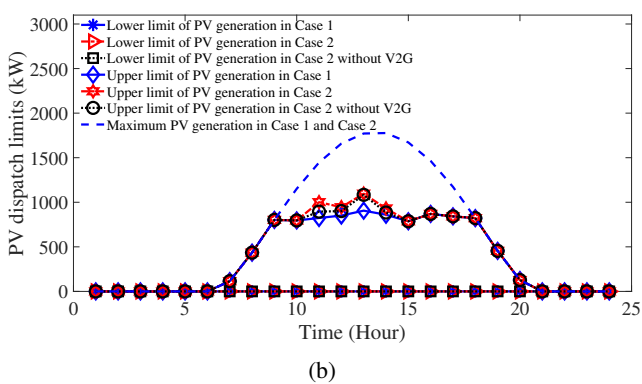
TABLE X: Characteristics of EV Clusters in the IEEE 123-Bus System

EV cluster	Number of vehicles	Bus	P^{max}	E^{min}	E^{max}
1	20	13	148	60	600
2	12	51	88.8	36	360
3	10	65	74	30	300
4	6	18	44.4	18	180
5	20	40	148	60	600
6	10	88	74	30	300

1) Case 1 - PV dispatch limits with forecasted PV generation and demand: In this case, the feasible dispatch limits for PV generation are determined while ignoring the EV interconnections to the network. The lower and upper limits for PV generation on phases A, B, and C are shown in Fig. 5a, Fig. 5b, and Fig. 5c respectively. As shown in these figures, once the PV generation is more than demand the excess PV generation is curtailed. At hour 13, the total real demand on phase A is 1405.80 kW; the PV generation units serve the load in this hour and the main distribution feeder and DGs serve 0 kW. The available PV generation at this hour is 1776.768 kW and the PV generation curtailment is 370.968 kW. The lower PV dispatch limits on phases A, B, and C are zero at all hours, which shows that the main distribution feeder and DGs can supply the demand on these phases.

2) Case 2 - PV dispatch limits with forecasted PV generation and demand, and the uncertainty in the EV interconnection: In this case, the maximum battery capacity of each EV is 30 kWh and the minimum capacity is 10% of maximum capacity. EVs can leave at the departure time with a fully charged battery and the forecasted available energy at arrival time is 25% of the maximum EV's battery capacity. The uncertainty sets for the maximum available energy in EV clusters 1-6 are [540, 600] kWh, [324, 360] kWh, [270, 300] kWh, [162, 180] kWh, [540, 600] kWh, and [270, 300] kWh respectively. The uncertainty sets for the minimum available energy for EV clusters 1-6 are [60,72] kWh, [36, 43.2] kWh, [30, 36] kWh, [18, 21.6] kWh, [60, 72]kWh, and [30, 36] kWh respectively. The uncertainty sets for the available energy at arrival time for EV clusters 1-6 are [120, 172.8] kWh, [72, 103.68] kWh, [60, 86.4]kWh, [36, 51.84] kWh, [120, 172.8] kWh, and [60, 86.4] kWh respectively. The uncertainty sets for the available energy at departure time for EV clusters 1-6 are [480, 600] kWh, [288, 360] kWh, [240, 300] kWh, [144, 180] kWh, [480,600] kWh, and [240,300] kWh respectively. The uncertainty sets for the maximum charging/discharging power dispatch for EV clusters 1-6 are [148, 207.2] kW,





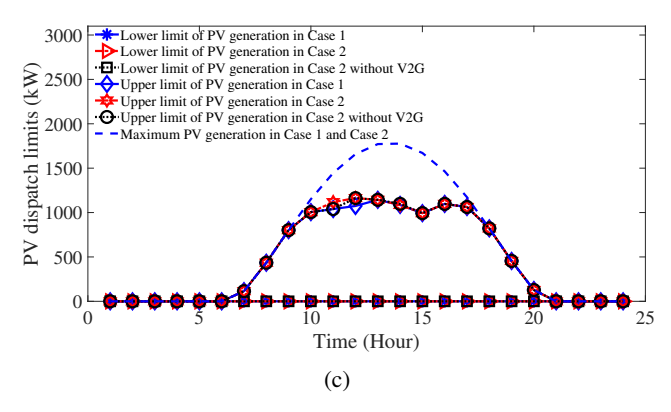


Fig. 5: The total PV's dispatch limits for (a) phase A, (b) phase B and (c) phase C in Case 1, and Case 2 with and without V2G.

[88.8, 124.32] kW, [74, 103.6] kW, [44.4, 62.16] kW, [148, 207.2] kW, and [74, 103.6] kW respectively. The uncertainty sets for arrival and departure times are similar to the previous case study. The impacts of V2G operation mode and the budget of uncertainty on the PV dispatch limits are investigated.

a) The impact of V2G operating mode on PV dispatch limits
Fig. 5 demonstrates the upper PV dispatch limits with and
without V2G capability of the EV clusters. As shown in this
figure, once the EVs are connected to the distribution network
the upper dispatch limits on all phases are increased compared
to Case 1. Table XI shows the total upper PV dispatch limit
on each phase. As shown in this table, the total upper dispatch
limits are increased with V2G capability compared to the case
in which EVs do not have V2G capability. Similar to Case

TABLE XI: Total Upper PV Dispatch Limits in Case 1 and Case 2 with and without V2G

Case	Phase A (kWh)	Phase B (kWh)	Phase C (kWh)
Case 1	12746.876	9358.380	11124.780
Case 2 (with V2G)	13377.627	10022.187	11422.419
Case 2 without V2G	13252.216	9813.846	11357.312

TABLE XII: Total Upper PV Dispatch Limits Considering the Budget of Uncertainty

	Total upper	limits on each	phase (kWh)
Scenarios	Phase A	Phase B	Phase C
1 (Case 2)	13377.627	10022.187	11422.419
2	13411.323	10063.659	11435.379
3	13445.019	10105.131	11431.467
4	13445.019	10105.131	11448.339
Case 1	12746.876	9358.380	11124.780

1, the total lower PV dispatch limits on all phases are zero which shows that the main distribution feeder and DGs are capable of supplying the demand. The solution is procured in 6 iterations once the V2G capability of EV clusters is considered.

b) The impact of the budget of uncertainty

Here, similar scenarios shown in Table IV are considered. For all scenarios, the minimum and maximum arrival and departure times are similar to the previous test case. Table XII shows the total upper dispatch limits of PV generation on phases A, B, and C. As shown in this table, the increase in the budget of uncertainty from 0% to 100% will decrease the total upper dispatch limits by 67.392 kW, 82.944 kW and 25.920 kW on phases A, B, and C respectively. Fig. 6a, Fig. 6b, and Fig. 6c demonstrate the effect of the budget of uncertainty on the hourly upper and lower PV dispatch limits on phases A, B, and C, respectively. Here, as the budget of uncertainty decreases the total upper dispatch limits will increase which means less total PV curtailment in the operation horizon. Furthermore, the lower dispatch limits are not affected by the budget of uncertainty. The worst-case realization of the arrival and departure times for the EV clusters are shown in Table XIV.

Similar to Table VI, the impacts of the budget of uncertainty for the arrival and departure times, i.e. $\Lambda^{\phi,arv}$ and $\Lambda^{\phi,dep}$, on the total upper PV dispatch limits are shown in Table XIII. Here, when the budget of uncertainty decreases from 100% to 0%, the total upper dispatch limits on phases A, B,

TABLE XIII: Total Upper PV Dispatch Limits with Budget of Uncertainty for Arrival/Departure Times

	Total upper	limits on each	phase (kWh)	Convergence
Scenarios	Phase A	Phase B	Phase C	Iteration
5	13377.627	9968.197	11422.419	6
6	13411.371	10042.433	11422.419	4
7	13421.494	10022.187	11448.747	3
8	13421.494	10076.177	11458.467	3
9	13421.494	10076.177	11469.291	2

TABLE XIV: Worst-Case Realization of Arrival and Departure Times in the IEEE 123-bus system

				Arriv	al and dep	parture tin	es for EV	clusters [hour]			
Scenario	$T_1^{a,arv}$	$T_1^{a,dep}$	$T_2^{b,arv}$	$T_2^{b,dep}$	$T_3^{c,arv}$	$T_3^{c,dep}$	$T_4^{a,arv}$	$T_4^{a,dep}$	$T_5^{b,arv}$	$T_5^{b,arv}$	$T_6^{c,arv}$	$T_6^{c,dep}$
1 (Case 2)	10	15	8	17	8	15	8	17	10	15	8	15
2	8	17	8	15	8	15	10	17	8	15	8	15
3	10	17	10	15	10	17	10	15	10	17	10	15
4	10	17	10	15	10	17	10	15	10	17	10	15

 \uparrow Upper limit with $\Gamma^{\phi,(.)}=0$

Maximum PV generation

 \leftarrow Upper limit with $\Gamma^{\phi,(.)}=0$

-□ Lower limit in Case 2

dep=0 - - Maximum PV generation

-□- Lower limit in Case 2

,dep=0

Time (Hour)

(a)

Lower limit with $\Gamma^{\phi, \text{Emin}} = 0$, $\Gamma^{\phi, \text{Emax}} = 0$, and $\Gamma^{\phi, \text{arv}} = 0$, $\Gamma^{\phi, \text{dep}} = 0$ Upper limit in Case 2

Time (Hour)

(b)

and C increase by $43.867\ kW$, $107.98\ kW$, and $46.872\ kW$ respectively. Table XIII, also shows the number of iterations in which the proposed algorithm converged. It is worth noting that as the number of uncertain variables (i.e. the available energy at arrival and departure times, the maximum and minimum energy and power capacity of the EV clusters, and the arrival and departure times of the EV clusters) increases,

Lower limit with $\Gamma^{\phi,\text{Emin}}=0$, $\Gamma^{\phi,\text{Emax}}=0$

Upper limit with $\Gamma^{\phi,\text{Emin}}=0$, $\Gamma^{\phi,\text{Emax}}=0$

* Lower limit with $\Gamma^{\phi, \text{Emin}} = 0$, $\Gamma^{\phi, \text{Emax}} = 0$

Upper limit with $\Gamma^{\phi,\text{Emin}}=0$, $\Gamma^{\phi,\text{Emax}}=0$

 \Diamond Lower limit with $\Gamma^{\phi,(.)}=0$

rightharpoonup Upper limit with $\Gamma^{\phi, \text{Emin}} = 0$, $\Gamma^{\phi, \text{Emax}} = 0$, and $\Gamma^{\phi, \text{arv}} = 0$, $\Gamma^{\phi} = 0$

 \diamondsuit Lower limit with $\Gamma^{\phi,(.)}=0$

PV dispatch limits (kW,

PV dispatch limits (kW

1500

2000

1500

1000

Lower limit with $\Gamma^{\phi, \text{Emin}} = 0$, $\Gamma^{\phi, \text{Emax}} = 0$, and $\Gamma^{\phi, \text{Emin}} = 0$

⇔ Upper limit with $\Gamma^{\phi, \text{Emin}}$ =0, $\Gamma^{\phi, \text{Emax}}$ =0, and $\Gamma^{\phi, \text{arv}}$ =0, Γ^{ϕ}

the number of constraints formed by using the McCormick envelopes increases. This will increase the number of iterations and the solution time. Table XV shows the simulation times and the number of iterations for scenarios shown in Table XII for the IEEE 123-bus system.

V. CONCLUSION

This paper presents a framework to quantify the dispatch limits for the PV generation in the unbalanced distribution networks with EV interconnection. The presented framework captures the uncertainties associated with the interconnection of EVs, the available energy at arrival and departure times, as well as the uncertainty in power and energy capacity of the EV clusters. It is shown that integrating the EVs with no V2G will increase the lower or upper dispatch limit of the PV generation as the distribution feeder and DG capacities are limited, and the energy requirement for charging the EVs will increase the lower and upper PV dispatch limits. Moreover, the impact of the budget of uncertainty and the operating mode of EVs (V2G and non-V2G) on the dispatch limits of the PV generation, are investigated. It is shown that increasing the budget of uncertainty for EVs will increase the total lower dispatch limits or decrease the total upper dispatch limits of PV generation in the day-ahead operation. Moreover, V2G reduces the total lower dispatch limits or increases the total upper dispatch limits of PV generation. To capture the uncertainty associated with maximum forecasted PV generation and demand, a scenario-based approach is used to determine the upper and lower dispatch limits of the PV generation. The worst-case realization of the EV interconnection parameters is considered in each scenario and the expected lower and upper PV dispatch limits are calculated.

Future research in this domain could focus on datadriven approaches based on a limited number of observed samples to quantify the uncertainty associated with the EV interconnection and determine the upper and lower dispatch limits of PV generation. Such approaches could capture distribution network loss to quantify the locational PV dispatch limits in the distribution network.

2500

Lower limit with Γ^{φ,Emin}=0, Γ^{φ,Emax}=0

Upper limit with Γ^{φ,Emin}=0, Γ^{φ,Emax}=0

Lower limit in Case 2

Down limit with Γ^{φ,Emin}=0, Γ^{φ,Emax}=0, and Γ^{φ,arv}=0, Γ^{φ,dep}=0

Upper limit in Case 2

Upper limit with Γ^{φ,Emin}=0, Γ^{φ,Emax}=0, and Γ^{φ,arv}=0, Γ^{φ,dep}=0

Upper limit in Case 2

Upper limit with Γ^{φ,Emin}=0, Γ^{φ,Emax}=0, and Γ^{φ,arv}=0, Γ^{φ,dep}=0

Upper limit with Γ^{φ,C,0}=0

Lower limit with Γ^{φ,Emin}=0, Γ^{φ,Emax}=0, and Γ^{φ,arv}=0, Γ^{φ,dep}=0

Upper limit with Γ^{φ,C,0}=0

Lower limit with Γ^{φ,C,0}=0

Upper limit with Γ^{φ,C,0}=0

Lower limit with Γ^{φ,Emin}=0, Γ^{φ,Emax}=0, and Γ^{φ,arv}=0, Γ^{φ,dep}=0

Upper limit with Γ^{φ,C,0}=0

Lower limit with Γ^{φ,C,0}=0

Upper limit with Γ^{φ,C,0}=0

Lower limit with Γ^{φ,Emin}=0, Γ^{φ,Emax}=0, and Γ^{φ,arv}=0, Γ^{φ,dep}=0

Upper limit with Γ^{φ,C,0}=0

Lower limit with Γ^{φ,C,0}=0

Upper limit with Γ^{φ,Emin}=0

Fig. 6: The impact of budget of uncertainty on the PV dispatch limits on (a) phase A, (b) phase B and (c) phase C.

TABLE XV: Simulation time of scenarios in Tables XIV and IV for the IEEE 123-bus system

Scenario	Simulation time (hr: min)	Iteration
1 (Case 2)	3:55	6
2	3:13	5
3	2:38	4
4	3:06	5
Case 1	0:33	2

REFERENCES

- I. R. E. Agency, "Future of solar photovoltaic: deployment, investment, technology, grid integration and socio-economic aspects," A Global Energy Transformation, 2019.
- [2] "Global ev outlook 2019," International Energy Agency, Paris, 2019.[Online]. Available: https://www.iea.org/reports/global-ev-outlook-2019
- [3] J. Zhao, J. Wang, Z. Xu, C. Wang, C. Wan, and C. Chen, "Distribution network electric vehicle hosting capacity maximization: A chargeable region optimization model," *IEEE Transactions on Power Systems*, vol. 32, no. 5, pp. 4119–4130, 2017.
- [4] O. Hafez and K. Bhattacharya, "Integrating ev charging stations as smart loads for demand response provisions in distribution systems," *IEEE Transactions on Smart Grid*, vol. 9, no. 2, pp. 1096–1106, 2016.
- [5] P. Papadopoulos, S. Skarvelis-Kazakos, I. Grau, L. M. Cipcigan, and N. Jenkins, "Predicting electric vehicle impacts on residential distribution networks with distributed generation," in 2010 IEEE Vehicle Power and Propulsion Conference. IEEE, 2010, pp. 1–5.
- [6] M. H. Amini, M. P. Moghaddam, and O. Karabasoglu, "Simultaneous allocation of electric vehicles' parking lots and distributed renewable resources in smart power distribution networks," *Sustainable cities and society*, vol. 28, pp. 332–342, 2017.
- [7] L. Hua, J. Wang, and C. Zhou, "Adaptive electric vehicle charging coordination on distribution network," *IEEE Transactions on Smart Grid*, vol. 5, no. 6, pp. 2666–2675, 2014.
- [8] K. Coogan, M. J. Reno, S. Grijalva, and R. J. Broderick, "Locational dependence of pv hosting capacity correlated with feeder load," in 2014 IEEE PES T&D Conference and Exposition. IEEE, 2014, pp. 1–5.
- [9] A. Navarro-Espinosa and L. F. Ochoa, "Increasing the pv hosting capacity of lv networks: Oltc-fitted transformers vs. reinforcements," in 2015 IEEE Power & Energy Society Innovative Smart Grid Technologies Conference (ISGT). IEEE, 2015, pp. 1–5.
- [10] S. Sakar, M. E. Balci, S. H. A. Aleem, and A. F. Zobaa, "Increasing pv hosting capacity in distorted distribution systems using passive harmonic filtering," *Electric Power Systems Research*, vol. 148, pp. 74–86, 2017.
- [11] F. Ding and B. Mather, "On distributed pv hosting capacity estimation, sensitivity study, and improvement," *IEEE Transactions on Sustainable Energy*, vol. 8, no. 3, pp. 1010–1020, 2016.
- [12] S. Hashemi and J. Østergaard, "Efficient control of energy storage for increasing the pv hosting capacity of lv grids," *IEEE Transactions on Smart Grid*, vol. 9, no. 3, pp. 2295–2303, 2016.
- [13] S. Hashemi, J. Østergaard, T. Degner, R. Brandl, and W. Heckmann, "Efficient control of active transformers for increasing the pv hosting capacity of lv grids," *IEEE Transactions on Industrial Informatics*, vol. 13, no. 1, pp. 270–277, 2016.
- [14] A. Dubey and S. Santoso, "On estimation and sensitivity analysis of distribution circuit's photovoltaic hosting capacity," *IEEE Transactions* on *Power Systems*, vol. 32, no. 4, pp. 2779–2789, 2016.
- [15] R. Torquato, D. Salles, C. O. Pereira, P. C. M. Meira, and W. Freitas, "A comprehensive assessment of pv hosting capacity on low-voltage distribution systems," *IEEE Transactions on Power Delivery*, vol. 33, no. 2, pp. 1002–1012, 2018.
- [16] S. Lakshmi and S. Ganguly, "Modelling and allocation planning of voltage-sourced converters to improve the rooftop pv hosting capacity and energy efficiency of distribution networks," *IET Generation*, *Transmission & Distribution*, vol. 12, no. 20, pp. 4462–4471, 2018.
- [17] R. Mahroo-Bakhtiari, M. Izadi, A. Safdarian, and M. Lehtonen, "Distributed load management scheme to increase pv hosting capacity in lv feeders," *IET Renewable Power Generation*, vol. 14, no. 1, pp. 125–133, 2020.
- [18] J. F. Sousa, C. L. Borges, and J. Mitra, "Pv hosting capacity of lv distribution networks using smart inverters and storage systems: a practical margin," *IET Renewable Power Generation*, vol. 14, no. 8, pp. 1332–1339, 2020.

- [19] S. Wang, Y. Dong, L. Wu, and B. Yan, "Interval overvoltage risk based pv hosting capacity evaluation considering pv and load uncertainties," *IEEE Transactions on Smart Grid*, vol. 11, no. 3, pp. 2709–2721, 2019.
- [20] A. Chaouachi, E. Bompard, G. Fulli, M. Masera, M. De Gennaro, and E. Paffumi, "Assessment framework for ev and pv synergies in emerging distribution systems," *Renewable and Sustainable Energy Reviews*, vol. 55, pp. 719–728, 2016.
- [21] H. Kikusato, Y. Fujimoto, S.-i. Hanada, D. Isogawa, S. Yoshizawa, H. Ohashi, and Y. Hayashi, "Electric vehicle charging management using auction mechanism for reducing pv curtailment in distribution systems," *IEEE Transactions on Sustainable Energy*, vol. 11, no. 3, pp. 1394–1403, 2019.
- [22] Y. Guo, J. Xiong, S. Xu, and W. Su, "Two-stage economic operation of microgrid-like electric vehicle parking deck," *IEEE Transactions on Smart Grid*, vol. 7, no. 3, pp. 1703–1712, 2015.
- [23] K. Mahmud, M. J. Hossain, and G. E. Town, "Peak-load reduction by coordinated response of photovoltaics, battery storage, and electric vehicles," *IEEE Access*, vol. 6, pp. 29 353–29 365, 2018.
- [24] Z. Akhtar, M. Opatovsky, B. Chaudhuri, and S. Y. R. Hui, "Comparison of point-of-load versus mid-feeder compensation in lv distribution networks with high penetration of solar photovoltaic generation and electric vehicle charging stations," *IET Smart Grid*, vol. 2, no. 2, pp. 283–292, 2019.
- [25] S. Weckx and J. Driesen, "Load balancing with ev chargers and pv inverters in unbalanced distribution grids," *IEEE transactions on Sustainable Energy*, vol. 6, no. 2, pp. 635–643, 2015.
- [26] C. Sabillon, J. F. Franco, M. J. Rider, and R. Romero, "Joint optimal operation of photovoltaic units and electric vehicles in residential networks with storage systems: A dynamic scheduling method," *International Journal of Electrical Power & Energy Systems*, vol. 103, pp. 136–145, 2018.
- [27] M. R. Islam, H. Lu, G. Fang, L. Li, and M. J. Hossain, "Optimal dispatch of electrical vehicle and pv power to improve the power quality of an unbalanced distribution grid," in 2019 International Conference on High Performance Big Data and Intelligent Systems (HPBD&IS). IEEE, 2019, pp. 258–263.
- [28] R. Fachrizal, U. H. Ramadhani, J. Munkhammar, and J. Widén, "Combined pv-ev hosting capacity assessment for a residential lv distribution grid with smart ev charging and pv curtailment," Sustainable Energy, Grids and Networks, vol. 26, p. 100445, 2021.
- [29] J. Zhao, T. Zheng, and E. Litvinov, "Variable resource dispatch through do-not-exceed limit," *IEEE Transactions on Power Systems*, vol. 30, no. 2, pp. 820–828, 2014.
- [30] Z. Li, F. Qiu, and J. Wang, "Data-driven real-time power dispatch for maximizing variable renewable generation," *Applied energy*, vol. 170, pp. 304–313, 2016.
- [31] ——, "Multi-period do-not-exceed limit for variable renewable generation dispatch considering discrete recourse controls," arXiv preprint arXiv:1608.05273, 2016.
- [32] M. Feizi and M. Khodayar, "Dispatchability limits for pv generation in unbalanced distribution network with evs," in *IEEE Power and Energy* Society General Meeting (PESGM). IEEE, 2020, pp. 1–5.
- [33] B. Chen, C. Chen, J. Wang, and K. L. Butler-Purry, "Sequential service restoration for unbalanced distribution systems and microgrids," *IEEE Transactions on Power Systems*, vol. 33, no. 2, pp. 1507–1520, 2017.
- [34] X. Chen, W. Wu, and B. Zhang, "Robust restoration method for active distribution networks," *IEEE Transactions on Power Systems*, vol. 31, no. 5, pp. 4005–4015, 2015.
- [35] J. Luedtke, M. Namazifar, and J. Linderoth, "Some results on the strength of relaxations of multilinear functions," *Mathematical programming*, vol. 136, no. 2, pp. 325–351, 2012.
- [36] G. Tal, M. A. Nicholas, J. Davies, and J. Woodjack, "Charging behavior impacts on electric vehicle miles traveled: who is not plugging in?" *Transportation Research Record*, vol. 2454, no. 1, pp. 53–60, 2014.